PHYSICAL REVIEW B **91**, 155138 (2015)

Atomically thin dilute magnetism in Co-doped phosphorene

L. Seixas,[1,*] A. Carvalho,[1] and A. H. Castro Neto[1,2]
[1]*Centre for Advanced 2D Materials and Graphene Research Centre, National University of Singapore, Singapore 117542, Singapore*
[2]*Boston University, 590 Commonwealth Avenue, Boston, Massachusetts 02215, USA*

(Received 25 February 2015; published 23 April 2015)

Two-dimensional dilute magnetic semiconductors can provide fundamental insights into the very nature of magnetic order and their manipulation through electron and hole doping. Besides the fundamental interest, due to the possibility of control of charge density, they can be extremely important in spintronics applications such as spin valve and spin-based transistors. In this paper, we studied a two-dimensional dilute magnetic semiconductor consisting of a phosphorene monolayer doped with cobalt atoms in substitutional and interstitial defects. We show that these defects can be stabilized and are electrically active. Furthermore, by including holes or electrons by a potential gate, the exchange interaction and magnetic order can be engineered, and may even induce a ferromagnetic-to-antiferromagnetic phase transition in p-doped phosphorene. At a Co concentration of 2.7%, we estimate a Curie temperature of $T_C^{MFA} = 466$ K in the mean-field approximation.

DOI: 10.1103/PhysRevB.91.155138 PACS number(s): 73.61.Cw, 75.30.Hx, 75.50.Mm

I. INTRODUCTION

Over the last decades the field of dilute magnetic semiconductors (DMSs) has seen important developments [1–8], both in fundamental aspects and prospective technological applications. As for the fundamental aspects, it was possible to understand the mechanisms of interaction between diluted magnetic impurities allowing ferromagnetic semiconductors at room temperature [7,8]. From the point of view of prospective applications, the marriage between the world of two-dimensional semiconductors and the world of magnetic data storage could provide us two-dimensional spintronics devices such as nonvolatile magnetoresistive memories, spin valve, spin-based transistors, and even magnetically enhanced optoelectronics devices [9].

Theoretical works based upon first-principles calculations have greatly contributed to the understanding of magnetism in dilute semiconductor materials [4,5]. Furthermore, it has been possible to achieve a spontaneous magnetic order above room temperature in a few classes of materials, including magnetic semiconducting oxides and nitrides [6,8]. However, in practice disorder effects and thermal fluctuations result in Curie temperatures well below the expectations.

In parallel, despite the success of two-dimensional (2D) materials such as graphene [10,11], transition metal dichalcogenides (TMDs) [12,13], and phosphorene, magnetism in 2D semiconductors has remained almost unexplored. One of the reasons for this might have been a theoretical result [14] indicating that the Curie temperature in 2D DMS tends to be substantially lower than for the corresponding 3D system. However, a subsequent work dissipated doubts by showing that including an adequate description of the disorder and the temperature dependence of the Fermi energy, it is possible to achieve much higher transition temperatures [15]. Concordantly, a Monte Carlo study of Mn-doped MoS_2, with first-principles parameters, has unraveled the potential of monolayer materials by predicting Curie temperatures above room temperature [16].

From a technical point of view, 2D semiconductors have other winning factors that can be explored in magnetic or spintronic devices. First, the carrier concentration can be controlled externally by gating. And there is room for improving the control over the impurity concentration, for example by exploring the possibility of using adatoms to incorporate impurities in concentrations above the solubility limit. In practice, studies of magnetic semiconductor nanostructures with lower dimensionalities, including semiconductor nanocrystals and nanowires [6,17–21] doped with transition metals (TMs) indicate that improved control of magnetic dopants can be used to increase the Curie temperature.

Phosphorene [22–24], a monolayer of black phosphorus, presents some advantages compared with other previously studied 2D semiconductors. Different from semiconducting TMDs, it is an elemental semiconductor and therefore less prone to vacancies [25]. Further, it has an anisotropic structure allowing in principle for different exchange interaction strength along the two principal directions. In host heteropolar semiconductors such as GaAs (zinc-blende structure) doped with transition metals, the Curie temperature is reduced by antisite defects [4]. It is expected that in 2D heteropolar semiconductors such as TMDs, antisite defects [26] will result in the same effect. However, in elemental host semiconductors such as phosphorene, this kind of defect does not exist. Thus, Curie temperatures of dilute magnetic semiconductors based on phosphorene are likely to be higher than those found in TM-doped TMDs.

In this paper, we use Co as a prototype magnetic impurity to show that it is possible to achieve magnetism (ferromagnetism and antiferromagnetism) in phosphorene and that this can be switched by the gate voltage through the control of the carrier density. We first studied the stability and electronic properties of Co defects in phosphorene (interstitial and substitutional), and thereafter, the magnetic orders acquired through the long-range interaction between diluted Co defects.

II. METHODS

Electronic, energetic, and magnetic properties of the systems studied were calculated via first-principles methods based

---

[*] seixasle@gmail.com

upon density functional theory (DFT) [27,28]. The simulations were performed with the VASP code (Vienna *Ab initio* Simulation Package) [29,30] with external potentials in projector augmented-wave (PAW) approximation [31] and exchange-correlation functional in generalized gradient approximation Perdew-Burke-Ernzerhof approximation (GGA-PBE) [32] and Heyd-Scuseria-Ernzerhof approximation (HSE06) [33]. The primitive unit cell for pristine phosphorene in our calculations is characterized by lattice constants $a \approx 3.298$ Å and $b \approx 4.625$Å. We use vacuum distances of 15 Å to avoid spurious interactions. We use a cutoff energy of 400 eV for Kohn-Sham orbitals and sampled the Brillouin zone using a $5\times5\times1$ grid generated with Monkhorst-Pack algorithm [34] for a 5×4 supercell. For density of states (DOS) and projected density of states (PDOS), we use a $15\times15\times1$ grid for Brillouin-zone integrations. The geometries are relaxed with residual force criteria of 10^{-3} eV/Å. For the calculation of magnetic anisotropy energies (MAEs), we use noncollinear spin polarization in a fully relativistic framework. Volumetric data are analyzed with the VESTA program [35].

Ionization levels are calculated using the marker method [36], taking the pristine supercell as reference. This method was found to give similar results to ionization levels calculated using the formation energy method, after correcting for spurious electrostatic interactions, which partially cancel when systems with the same charge are compared [37].

III. COBALT POINT DEFECTS

Cobalt atoms can either be adsorbed on phosphorene or occupy a substitutional position (Fig. 1). Both of them lead to very small lattice distortion. Substitutional cobalt ($\mathrm{Co_P}$) forms three bonds, 3–5% shorter than the original P-P bonds [Fig. 1(a)]. Interstitial (or adsorbed) cobalt ($\mathrm{Co_i}$) also forms three bonds, connecting P atoms in two zigzag ridges on the same side of the layer [Fig. 1(b)]. The adsorption energy of $\mathrm{Co_i}$ defect is among the highest of TM adatoms on phosphorene [38].

In order to calculate the electronic properties of an isolated Co point defect in phosphorene, a 5×4 supercell is used, so that these Co point defects are diluted in concentrations of 1.23% (interstitial) and 1.25% (substitutional). Unless otherwise stated, all the calculations described in this paper are in these concentrations. Whereas the $\mathrm{Co_P}$-doped phosphorene does not present nonzero magnetic moments, the $\mathrm{Co_i}$-doped phosphorene presents a total magnetic moment of $m = 1\mu_\mathrm{B}$. This is 0.12 eV lower in energy than the nonmagnetic state (NM).

The magnetic anisotropy energy (MAE) for the diluted $\mathrm{Co_i}$ defect is obtained from fully relativistic and noncollinear spin-polarized calculations. The vertical spin polarization (z direction) proved to be the lowest energy, whereas spin polarizations in other directions (x and y direction) are related by $\mathrm{MAE}(yz) = 1.0$ meV, $\mathrm{MAE}(xz) = 0.8$ meV, and $\mathrm{MAE}(xy) = 0.2$ meV. Since the magnetic anisotropy is small, we will treat the magnetic impurities using a collinear spin-polarized density-functional formalism.

A. Electronic band structures

The band structures calculated for pristine, $\mathrm{Co_P}$-doped and $\mathrm{Co_i}$-doped phosphorene are shown in Figs. 1(c)–1(f). For

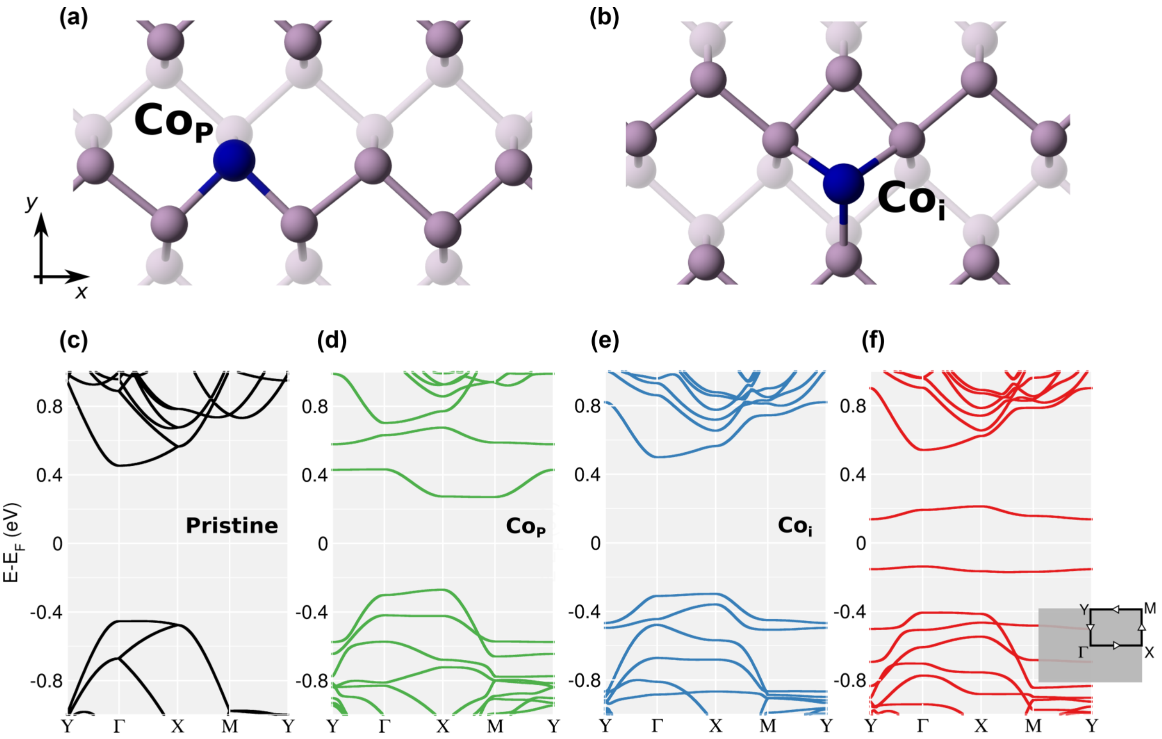

FIG. 1. (Color online) Ball-and-stick representation of phosphorene with (a) substitutional Co ($\mathrm{Co_P}$) defect and (b) interstitial (or adsorbed) Co ($\mathrm{Co_i}$) defect. Electronic band structures for (c) pristine phosphorene, (d) $\mathrm{Co_P}$-doped phosphorene, (e),(f) $\mathrm{Co_i}$-doped phosphorene for spin up and down, respectively. The Fermi level is set at zero.

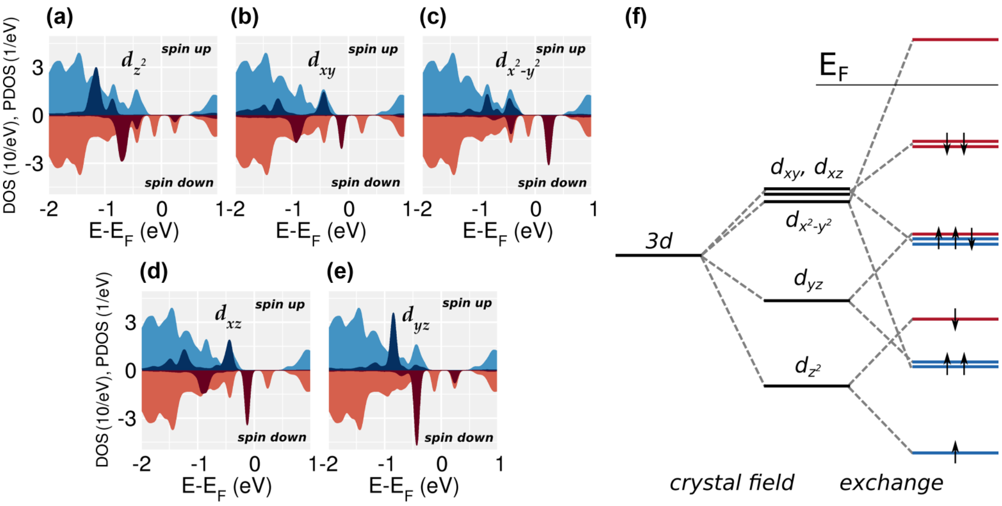

FIG. 2. (Color online) (a)–(e) Density of states (DOS) shown as light blue and light red areas, and projected density of states (PDOS) on cobalt atoms shown as dark blue and dark red areas. The PDOS are decomposed on atomic orbitals: (a) d_{z^2}, (b) d_{xy}, (c) $d_{x^2-y^2}$, (d) d_{xz}, and (e) d_{yz}. The DOS scale is ten times larger than the PDOS scale. (f) Schematic representation of 3d level splitting in crystal field with C_s point symmetry and exchange interaction.

the spin-degenerated Co$_\mathrm{P}$-doped phosphorene band structure [shown in Fig. 1(d)], defect levels with dispersion of approximately 0.2 eV were introduced at about midgap, and the valence band shifts in such way that the valence-band maximum (VBM) becomes located at the X point. This shift in VBM will suppress the luminescence of phosphorene [23,39]. As for the band structures (spin up and down) of Co$_\mathrm{i}$-doped phosphorene, two localized levels are introduced in the spin-down channel. One is occupied (below the Fermi level) and other unoccupied (above the Fermi level). For the spin-up channel, all Co d states are occupied, leading to a spin imbalance resulting in a local magnetic moment of $1\mu_\mathrm{B}$, which gives rise to a macroscopic magnetization.

B. Origin of the defect state

The origin of the local magnetic moment in Co$_\mathrm{i}$-doped phosphorene can be understood by analyzing the crystal-field splitting, the hybridization between the Co valence states ($4s^2 3d^7$), and the phosphorene host states, which have mainly s and p character.

From the symmetry breaking point of view, while pristine phosphorene has C_{2v} point symmetry, cobalt point defects reduce the symmetry to C_s. Only a mirror plane, passing through the defect and perpendicular to phosphorene, is preserved. In this lower symmetry, cobalt d orbitals transform as $3A' \oplus 2A''$, where d_{xy}, $d_{x^2-y^2}$, and d_{z^2} belong to the A' representation, and d_{xz} and d_{yz} belong to the A'' representation [40]. Phosphorus p orbitals split in $2A' \oplus A''$, where p_x and p_y are in A' representation, and p_z is in A'' representation. We observe that the pd hybridization occurs in A' with p_x, p_y, d_{xy}, and $d_{x^2-y^2}$ orbitals, and in A'' with p_z and d_{xz}.

Different from interstitial transition metals in other materials, the hybridization is quite strong and therefore the electronic states cannot be understood based only on a crystal-field-splitting model. This is apparent in the projected density of states (PDOS) on cobalt atoms, obtained from the decomposition on atom-centered real spherical harmonics, shown in Figs. 2(a)–2(e). We notice that there is pd hybridization between p orbitals from phosphorene and d orbitals from cobalt defects, resulting in bonding and antibonding hybrid states. The exchange field splits each of these states, leading to a splitting into four peaks for each d orbital. This effect is more pronounced on d_{xy}, d_{xz}, and $d_{x^2-y^2}$ orbitals, which have maximum amplitude in the xy plane [Figs. 2(b)–2(d)]. The d_{z^2} and d_{yz} orbitals are nodal at the xy plane and therefore undergo smaller hybridization and have lower energies. A schematic representation of crystal-field and exchange splitting is shown in Fig. 2(f). For simplicity, this takes into account only the states with highest d character for each d orbital type and spin. Whereas the d_{xz}, d_{yz}, d_{xy}, and d_{z^2} orbitals show exchange splitting in the range 0.32–0.45 eV, the $d_{x^2-y^2}$ orbital presents exchange splitting of approximately 1.08 eV. This large apparent exchange splitting is in fact a combined effect of pd hybridization and exchange field splitting, resulting in a higher peak for the spin-up bonding state and the spin-down antibonding state.

C. Formation energy

We define the formation energy for neutral defects (X^0) as [41]

$$E^f[X^0] = E_\mathrm{tot}[\mathrm{P}:X^0] - E_\mathrm{tot}[\mathrm{P}] - \mu_X - n_\mathrm{P}\mu_\mathrm{P}, \qquad (1)$$

where $E_\mathrm{tot}[\mathrm{P}:X^0]$ is the total energy of phosphorene with X^0 defect, $E_\mathrm{tot}[\mathrm{P}]$ is the total energy of pristine phosphorene, $\mu_X = \mu_\mathrm{Co}$ is the chemical potential of cobalt calculated from 3D crystal with hexagonal lattice, μ_P is the chemical potential of phosphorus calculated from pristine phosphorene. The number of phosphorus atoms missing (n_P) is $n_\mathrm{P} = 0$ for Co$_\mathrm{i}$ defects and $n_\mathrm{P} = -1$ for Co$_\mathrm{P}$ defects.

In the neutral charge state, substitutional cobalt defects have the lowest formation energy. While the formation energy of neutral Co$_\mathrm{P}$ is $E^f[\mathrm{Co_P}^0] = 1.20$ eV, neutral Co$_\mathrm{i}$ has $E^f[\mathrm{Co_i}^0] = 1.42$ eV. However, both defects are electrically active and therefore the formation energy depends on the Fermi

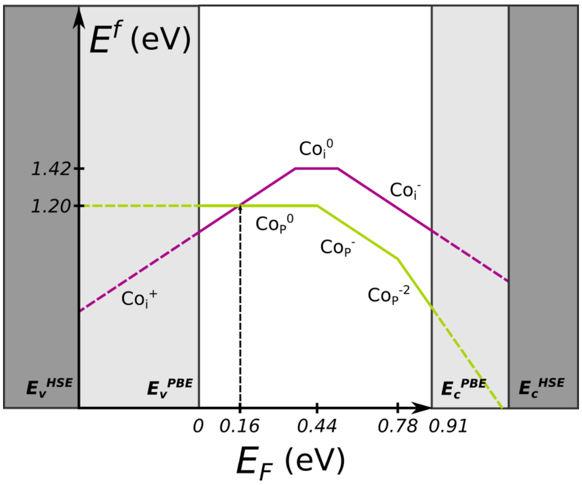

FIG. 3. (Color online) Formation energy vs Fermi level for charged and neutral states of Co_P (light green) and Co_i (dark violet) defects.

level E_F (Fig. 3). Calculating the thermodynamic ionization levels $I(+/0)$ and $I(0/-)$ with the marker method [36], we can evaluate the formation energies of charged point defects as a function of the Fermi level as

$$E^f[X^+](E_F) = E^f[X^0] - I(+/0) + E_F, \qquad (2)$$

for *positive* charged point defects (X^+), and

$$E^f[X^-](E_F) = \Delta_g^{PBE} + E^f[X^0] + I(0/-) - E_F \qquad (3)$$

for *negative* charged point defects (X^-), where the donor and acceptor levels are given relative to the valence- and conduction-band edges, respectively. The Fermi level is set to zero at VBM. In Eq. (3), Δ_g^{PBE} is the band gap at the PBE level. Substitutional Co is an acceptor with $I(0/-)$ level at midgap (at the PBE level) and a double acceptor at $E_F = 0.78$ eV, whereas Co_i is amphoteric. Thus, in p-type material Co_i is stabilized, becoming more energetically favorable than Co_P. According to the PBE calculations, this happens for E_F between E_v and $E_v + 0.16$ eV.

However, since the band gap is severely underestimated at the PBE level, we extrapolate the results using the valence- and conduction-band shifts obtained from HSE calculations for the pristine phosphorene. Here, we assume that the gap levels of Co_i and Co_P are very localized, and are not shifted with respect to the vacuum level by the exchange component [42]. By fixing the PBE and HSE vacuum level at the same energy, we observe the shifts $\Delta E_v = E_v^{HSE} - E_v^{PBE} = -0.48$ eV in the valence band, and $\Delta E_c = E_c^{HSE} - E_c^{PBE} = +0.31$ eV in the conduction band. The band gap increases from $\Delta_g^{PBE} = 0.91$ eV at the PBE level to $\Delta_g^{HSE} = 1.70$ eV at the HSE level. Because of this large shift in the valence band at the HSE level, the formation energy of the donor ${Co_i}^+$ can be up to 0.42 eV smaller than the formation energy of ${Co_P}^0$.

IV. MAGNETIC COUPLING AND ORDER

The pd hybridization in Co_i-doped phosphorene is characterized by long-range and anisotropic interactions between cobalt defects described in Fig. 4. In the armchair direction, the exchange interaction aligns the spin parallel for short distances and antiparallel for longer distances. In the zigzag direction the behavior of the exchange interaction is the opposite. These interactions have positive and negative exchange coupling with the distance and direction, leading to ferromagnetic and antiferromagnetic orders.

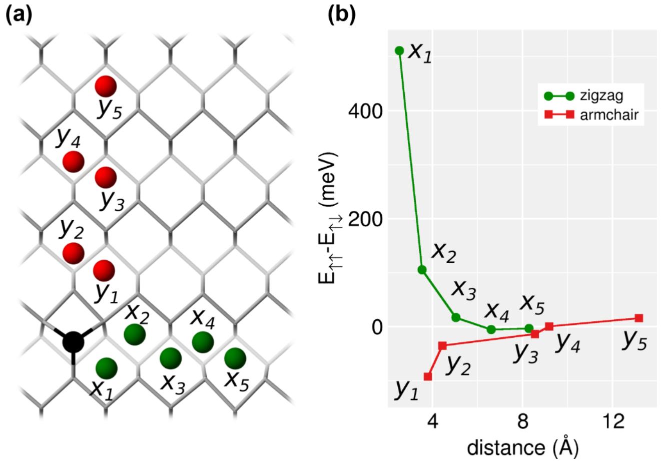

FIG. 4. (Color online) (a) Schematic representation of Co impurity sites along zigzag and armchair directions. (b) Energy differences between parallel ($E_{\uparrow\uparrow}$) and antiparallel spins ($E_{\uparrow\downarrow}$) as a function of distance and direction.

In order to determine the magnetic order of the fundamental state, we use a 4×4 supercell with four Co_i defects in equivalent positions. In these systems, the Co_i defects are diluted in a concentration of 5.88%. In a neutral system, the ferromagnetic (FM) order was more energetically favorable than antiferromagnetic (AFM) order by $\Delta E_{FM-AFM} = -24$ meV. These magnetic orders are shown in Figs. 5(a) and 5(b) by spin density ($s = \rho_\uparrow - \rho_\downarrow$) isosurfaces. Positive values of isosurfaces ($s = +2\times10^{-3}$ bohrs^{-3}) are shown in blue, and negative values ($s = -2\times10^{-3}$ bohrs^{-3}) are shown in red.

Since Co_i defects are amphoteric, they can accept or donate electrons. Doping the system with electrons or holes, we can change the interaction between defects, and therefore, change

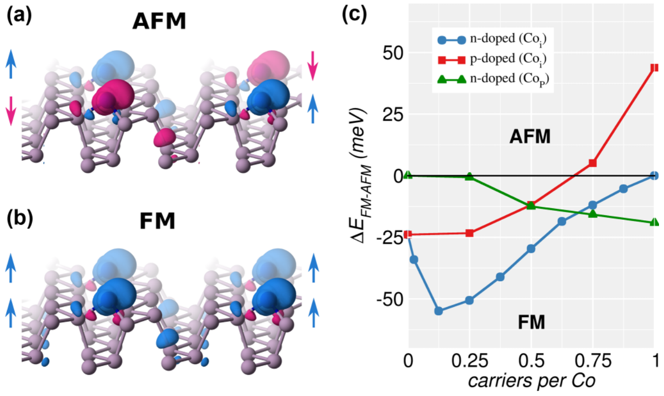

FIG. 5. (Color online) Spin density isosurfaces of $\pm2\times10^{-3}$ bohrs^{-3} for (a) antiferromagnetic (AFM) order, and (b) ferromagnetic (FM) order. Positive and negative values of isosurfaces are shown in different colors. (c) Energy difference between FM and AFM orders as function of carrier densities (electrons and holes) for n-doped Co_i (blue), p-doped Co_i (red), n-doped Co_P (green) defects.

the magnetic order of the system. We observe that when $\mathrm{Co_i}$-doped phosphorene is n-type, ΔE_{FM-AFM} decreases until a minimum value at $0.125e/\mathrm{Co}$ ($n = 1.7\times10^{13}/\mathrm{cm}^2$), and then increases until the ferromagnetic order is no longer stable at $1e/\mathrm{Co}$. For the p-type $\mathrm{Co_i}$-doped phosphorene, the difference ΔE_{FM-AFM} increases monotonically with the hole density, so that there is a phase transition from ferromagnetic to antiferromagnetic at a critical hole density ($p_c = 1.11\times10^{14}/\mathrm{cm}^2$).

In contrast, $\mathrm{Co_P}$ can only exist in the neutral, single negative and double negative charge states. Thus, a similar prototype system with four $\mathrm{Co_P}$ defects, the $\mathrm{Co_P}$-doped phosphorene, were studied doping the system with electrons. These systems begin from a nonmagnetic order at intrinsic state to a ferromagnetic order with $\Delta E_{FM-AFM} = -19$ meV at $1e/\mathrm{Co}$ ($n = 1.64\times10^{14}/\mathrm{cm}^2$). Similar electric-field control of magnetism was observed in (In,Mn)As quantum well [2].

Besides the system with four magnetic impurities in the 4×4 supercell, we also calculate the magnetic properties of these impurities in the 6×6 supercell. In this system, the Co concentration is approximately 2.7% and the energy difference $\Delta E_{FM-AFM} = -241$ meV. This result is counterintuitive, since at a lower Co concentration the energy difference ΔE_{FM-AFM} increases by a factor of 10. Based on this energy difference, we can estimate the Curie temperature in the mean-field approximation (MFA) via

$$\frac{3}{2}k_B T_C^{MFA} = -\frac{\Delta E_{FM-AFM}}{N_{imp}}, \tag{4}$$

where $N_{imp} = 4$ is the number of Co impurities in the supercell. The Curie temperature estimated is about $T_C^{MFA} = 466$ K, above room temperature.

V. CONCLUSION

In summary, we show that interstitial and substitutional cobalt defects in phosphorene are stable, and the lowest energy configurations are $\mathrm{Co_i}$ for p-type phosphorene and $\mathrm{Co_P}$ for intrinsic and n-type phosphorene. Also we show that through electron and hole doping which can be controlled by gate potential, the exchange interaction between impurities can be engineered to yield ferromagnetic or antiferromagnetic order. This effect can be used in prospective spintronic applications. Whereas TM-doped $\mathrm{MoS_2}$ has shown diluted magnetism with very high Curie temperatures (above room temperature) [16], dilute magnetic phosphorene presents some advantages due to absence of antisite defects and is less prone to vacancies, indicating potentially higher Curie temperatures and control of disordered impurities. For a Co impurity concentration of 2.7%, we estimate a Curie temperature of $T_C^{MFA} = 466$ K. Even including disorder effects, we can still expect that Co-doped phosphorene shows ferromagnetism above room temperature.

ACKNOWLEDGMENTS

L.S. acknowledges financial support provided by Conselho Nacional de Desenvolvimento Científico e Tecnológico (CNPq/Brazil). The authors acknowledge the National Research Foundation, Prime Minister's Office, Singapore, under its Medium Sized Centre Programme and CRP award "Novel 2D materials with tailored properties: Beyond graphene" (Grant No. R-144-000-295-281). The first-principles calculations were carried out on the Centre for Advanced 2D Materials (CA2DM) and Graphene Research Centre high-performance computing facilities.

[1] T. Dietl, H. Ohno, F. Matsukura, J. Cibert, and D. Ferrand, Zener model description of ferromagnetism in zinc-blende magnetic semiconductors, Science **287**, 1019 (2000).

[2] H. Ohno, D. Chiba, F. Matsukura, T. Omiya, E. Abe, T. Dietl, Y. Ohno, and K. Ohtani, Electric-field control of ferromagnetism, Nature (London) **408**, 944 (2000).

[3] H. Ohno, Making nonmagnetic semiconductors ferromagnetic, Science **281**, 951 (1998).

[4] K. Sato, L. Bergqvist, J. Kudrnovský, P. H. Dederichs, O. Eriksson, I. Turek, B. Sanyal, G. Bouzerar, H. Katayama-Yoshida, V. A. Dinh, T. Fukushima, H. Kizaki, and R. Zeller, First-principles theory of dilute magnetic semiconductors, Rev. Mod. Phys. **82**, 1633 (2010).

[5] A. Zunger, S. Lany, and H. Raebiger, The quest for dilute ferromagnetism in semiconductors: guides and misguides by theory, Physics **3**, 53 (2010).

[6] T. Dietl, A ten-years perspective on dilute magnetic semiconductors and oxides, Nat. Mater. **9**, 965 (2010).

[7] Y. Matsumoto, M. Murakami, T. Shono, T. Hasegawa, T. Fukumura, M. Kawasaki, P. Ahmet, T. Chikyow, S. Koshihara, and H. Koinuma, Room temperature ferromagnetism in transparent transition metal-doped titanium dioxide, Science **291**, 854 (2001).

[8] J. M. Coey, M. Venkatesan, and C. B. Fitzgerald, Donor impurity band exchange in dilute ferromagnetic oxides, Nat. Mater. **4**, 173 (2005).

[9] I. Žutić, J. Fabian, and S. Das Sarma, Spintronics: Fundamentals and applications, Rev. Mod. Phys. **76**, 323 (2004).

[10] K. S. Novoselov, A. K. Geim, S. Morozov, D. Jiang, Y. Zhang, S. Dubonos, I. Grigorieva, and A. Firsov, Electric field effect in atomically thin carbon films, Science **306**, 666 (2004).

[11] A. H. Castro Neto, F. Guinea, N. Peres, K. S. Novoselov, and A. K. Geim, The electronic properties of graphene, Rev. Mod. Phys. **81**, 109 (2009).

[12] K. S. Novoselov, D. Jiang, F. Schedin, T. Booth, V. Khotkevich, S. Morozov, and A. K. Geim, Two-dimensional atomic crystals, Proc. Natl. Acad. Sci. USA **102**, 10451 (2005).

[13] K. F. Mak, C. Lee, J. Hone, J. Shan, and T. F. Heinz, Atomically thin $\mathrm{MoS_2}$: A new direct-gap semiconductor, Phys. Rev. Lett. **105**, 136805 (2010).

[14] D. J. Priour Jr., E. H. Hwang, and S. Das Sarma, Quasi-two-dimensional diluted magnetic semiconductor systems, Phys. Rev. Lett. **95**, 037201 (2005).

[15] E. Z. Meilikhov and R. M. Farzetdinova, Quasi-two-dimensional diluted magnetic semiconductors with arbitrary carrier degeneracy, Phys. Rev. B **74**, 125204 (2006).

[16] A. Ramasubramaniam and D. Naveh, Mn-doped monolayer MoS_2: An atomically thin dilute magnetic semiconductor, Phys. Rev. B **87**, 195201 (2013).

[17] K. R. Kittilstved and D. R. Gamelin, Activation of high-T_C ferromagnetism in Mn^{2+}-doped ZnO using amines, J. Am. Chem. Soc. **127**, 5292 (2005).

[18] Y. Rao, H. Xu, Y. Liang, and S. Hark, Synthesis, microstructural and magnetic properties of mn-doped ZnO nanowires, Cryst. Eng. Commun. **13**, 2566 (2011).

[19] J. H. Park, M. G. Kim, H. M. Jang, S. Ryu, and Y. M. Kim, Co-metal clustering as the origin of ferromagnetism in co-doped ZnO thin films, Appl. Phys. Lett. **84**, 1338 (2004).

[20] C. Echeverría-Arrondo, J. Pérez-Conde, and A. Ayuela, Antiferromagnetic order in (Ga, Mn)N nanocrystals: A density functional theory study, Phys. Rev. B **82**, 205419 (2010).

[21] C. Echeverría-Arrondo, J. Pérez-Conde, and A. Ayuela, Antiferromagnetism in nanofilms of Mn-doped GaN, J. Phys. Chem. C **118**, 18064 (2014).

[22] A. S. Rodin, A. Carvalho, and A. H. Castro Neto, Strain-induced gap modification in black phosphorus, Phys. Rev. Lett. **112**, 176801 (2014).

[23] H. Liu, A. T. Neal, Z. Zhu, Z. Luo, X. Xu, D. Tománek, and P. D. Ye, Phosphorene: An unexplored 2d semiconductor with a high hole mobility, ACS Nano **8**, 4033 (2014).

[24] L. Li, Y. Yu, G. J. Ye, Q. Ge, X. Ou, H. Wu, D. Feng, X. H. Chen, and Y. Zhang, Black phosphorus field effect transistor, Nat. Nanotechnol. **9**, 372 (2014).

[25] Y. Liu, F. Xu, Z. Zhang, E. S. Penev, and B. I. Yakobson, Two-dimensional mono-elemental semiconductor with electronically inactive defects: the case of phosphorus, Nano Lett. **14**, 6782 (2014).

[26] W. Zhou, X. Zou, S. Najmaei, Z. Liu, Y. Shi, J. Kong, J. Lou, P. M. Ajayan, B. I. Yakobson, J.-C. Idrobo, Intrinsic structural defects in monolayer molybdenum disulfide, Nano Lett. **13**, 2615 (2013).

[27] P. Hohenberg and W. Kohn, Inhomogeneous electron gas, Phys. Rev. **136**, B864 (1964).

[28] W. Kohn and L. J. Sham, Self-consistent equations including exchange and correlation effects, Phys. Rev. **140**, A1133 (1965).

[29] G. Kresse and J. Furthmüller, Efficient iterative schemes for ab initio total-energy calculations using a plane-wave basis set, Phys. Rev. B **54**, 11169 (1996).

[30] G. Kresse and D. Joubert, From ultrasoft pseudopotentials to the projector augmented-wave method, Phys. Rev. B **59**, 1758 (1999).

[31] P. E. Blöchl, Projector augmented-wave method, Phys. Rev. B **50**, 17953 (1994).

[32] J. P. Perdew, K. Burke, and M. Ernzerhof, Generalized gradient approximation made simple, Phys. Rev. Lett. **77**, 3865 (1996).

[33] J. Heyd, G. E. Scuseria, and M. Ernzerhof, Hybrid functionals based on a screened Coulomb potential, J. Chem. Phys. **118**, 8207 (2003); **124**, 219906(E) (2006).

[34] H. J. Monkhorst and J. D. Pack, Special points for brillouin-zone integrations, Phys. Rev. B **13**, 5188 (1976).

[35] K. Momma and F. Izumi, VESTA 3 for three-dimensional visualization of crystal, volumetric and morphology data, J. Appl. Crystallogr. **44**, 1272 (2011).

[36] J. Coutinho, V. J. B. Torres, R. Jones, and P. R. Briddon, Electrical activity of chalcogen-hydrogen defects in silicon, Phys. Rev. B **67**, 035205 (2003).

[37] A. Carvalho and A. H. Castro Neto, Donor and acceptor levels in semiconducting transition-metal dichalcogenides, Phys. Rev. B **89**, 081406(R) (2014).

[38] V. V. Kulish, O. I. Malyi, C. Persson, and P. Wu, Adsorption of metal adatoms on single-layer phosphorene, Phys. Chem. Chem. Phys. **17**, 992 (2015).

[39] L. Seixas, A. S. Rodin, A. Carvalho, and A. H. Castro Neto, Exciton binding energy and luminescence in phosphorene under pressure, Phys. Rev. B **91**, 115437 (2015).

[40] M. Tinkham, *Group Theory and Quantum Mechanics* (McGraw-Hill, New York, 1964).

[41] C. Freysoldt, B. Grabowski, T. Hickel, J. Neugebauer, G. Kresse, A. Janotti, and C. G. van de Walle, First-principles calculations for point defects in solids, Rev. Mod. Phys. **86**, 253 (2014).

[42] A. Alkauskas, P. Broqvist, and A. Pasquarello, Defect energy levels in density functional calculations: Alignment and band gap problem, Phys. Rev. Lett. **101**, 046405 (2008).